Journal of Oceanology and Limnology
Vol. 40 No. 4, P. 1388-1403, 2022
https://doi.org/10.1007/s00343-021-1148-0

Petrology and geochemistry of cold seep carbonates from the northern Okinawa Trough, East China Sea: implications to early diagenesis*

Kehong YANG**, Zhimin ZHU, Yanhui DONG, Weiyan ZHANG, Fengyou CHU

Key Laboratory of Submarine Geosciences & Second Institute of Oceanography, Ministry of Natural Resources, Hangzhou 310012, China

Received Apr. 29, 2021; accepted in principle Jul. 13, 2021; accepted for publication Sep. 10, 2021

Abstract Carbonate samples were collected from the northern Okinawa Trough in the East China Sea in 2013. The petrology, mineralogy, carbon and oxygen isotopes, and rare earth elements (REEs) of these samples were analyzed. Aragonite, high-Mg calcite, and dolomite were the main carbonate minerals, the contents of which varied greatly among the carbonate samples. Petrological observations revealed the common occurrence of framboidal pyrites. The $\delta^{13}C$ values of carbonates varied from -53.7‰ to -39.3‰ (average of -47.3‰ based on Vienna Pee Dee Belemnite (V-PDB), n=9), and the $\delta^{18}O$ values ranged from 0.6‰ to 3.4‰ (average of 1.9‰; V-PDB, n=9). The carbon and oxygen isotope characteristics indicated that the carbonates precipitated during the anaerobic oxidation of methane. The carbon source was a mixture of thermogenic methane and biogenic methane, possibly with a greater contribution from the former. The oxygen isotope data showed that gas hydrate dissociation occurred during carbonate precipitation. The Ce anomalies suggested that the carbonates precipitated in an anoxic environment. A slight enrichment of middle REEs (MREEs) could be attributable to the early diagenesis. The structures, minerals, oxygen isotopes, and MREEs all indicated that the carbonates experienced some degree of early diagenesis. Therefore, the influence of early diagenesis should be considered when using geological and geochemical proxies to reconstruct original methane seepage environments.

Keyword: authigenic carbonate; carbon and oxygen isotopes; rare earth elements (REEs); anaerobic oxidation of methane (AOM); northern Okinawa Trough

1 INTRODUCTION

Authigenic carbonates have been reported to occur in areas of methane seepage on the seafloor along active and passive margins around the world (Campbell, 2006; Suess, 2014). Anaerobic oxidation of methane (AOM) and sulfate reduction are the dominant biogeochemical processes in methane seepages (e.g., Boetius et al., 2000). These processes lead to an increase in carbonate alkalinity because the production of bicarbonate favors the precipitation of authigenic carbonates:

$$CH_4+SO_4^{2-}\rightarrow HCO_3^-+HS^-+H_2, \quad (1)$$

$$2HCO_3^-+Ca^{2+}\leftrightarrow CaCO_3+CO_2+H_2O. \quad (2)$$

Authigenic carbonates provide important archives of methane seepages throughout geological history (e.g., Campbell, 2006; Suess, 2014; and references therein). Therefore, studies on authigenic carbonates can be used to reconstruct paleoenvironments and geochemical processes, and to discuss the formation and dissociation of gas hydrates, of which the main component is methane. However, the influence of early diagenesis should be taken into account when using cold seep carbonates to trace the geological history of methane seepages.

Diagenesis begins when carbonate minerals are formed (James and Choquette, 1983). During diagenesis, authigenic carbonates are susceptible to isotopic and elemental exchanges with diagenetic

* Supported by the National Natural Science Foundation of China (Nos. 41476050, 41106047)
** Corresponding author: yangkh@sio.org.cn

fluids (e.g., burial fluids, meteoric fluids, and dolomitization fluids) (Wang et al., 2018), which affect the accuracy of the initial conditions of seeping fluids reconstructed using authigenic carbonates. Swart (2015) summarized the study of carbonate diagenesis, and pointed out that isotopes (e.g., C, O, Sr, Mg, and Ca) and minor and trace elements (e.g., Ba, Li, U, and rare earth elements (REEs)) can be used to constrain diagenesis.

In cold seeps, minerals can be transformed, dissolved, and recrystallized during the early diagenesis of authigenic carbonates. For instance, aragonite and high-Mg calcite (HMC) can transform into low Mg-calcite (LMC) during early diagenesis (Joseph et al., 2013). In addition, aragonite can also recrystallize to different degrees, such as from microcrystalline to microspar (Feng et al., 2009b). Authigenic aragonite and Mg-calcite are the most common diagenetic carbonate phases observed in seep carbonates (Pierre and Fouquet, 2007; Crémière et al., 2016). Pyrites are also diagenetic minerals that are commonly observed in association with authigenic carbonates from cold seeps (Pierre, 2017), and can provide diagnostic information on the chemistry of the corresponding diagenetic fluids. The transformation of primary aragonite to calcite due to a change in the porewater composition during the late stage of early diagenesis may significantly modify the elemental composition of authigenic minerals (Zwicker et al., 2018).

Stable carbon and oxygen isotopes are commonly used as geochemical tracers to unravel the diagenetic history of carbonates (Swart, 2015). The $\delta^{18}O$ values of carbonates decrease with increasing age, whereas the $\delta^{13}C$ values are generally less influenced by diagenesis and more a reflection of primary changes in the global carbon cycle through time, because the factors controlling their fractionation are different (Swart, 2015). In cold seeps, the $\delta^{18}O$ values decrease over time due to post-depositional dissolution, as shown by several studies (e.g., Joseph et al., 2013; Tong et al., 2016). However, the $\delta^{13}C$ values can increase over time during diagenesis if secondary carbonates form in deep $\delta^{13}C$-enriched diagenetic or meteoric fluids (Joseph et al., 2013; Tong et al., 2016). The $\delta^{18}O$ values of carbonates are dependent upon both the temperature and $\delta^{18}O$ value of the fluid, but direct evidence of either the temperature or composition of the fluids is required (Swart, 2015). The correlation between $\delta^{13}C$ and $\delta^{18}O$ values can change during early diagenesis, and the covariation between these parameters can indicate the factors influencing diagenesis (Swart and Oehlert, 2018).

In cold seeps, REEs in methane-related carbonates are most commonly used to determine the fluid sources and changes in redox conditions within diagenetic environments (Zwicker et al., 2018, and the references therein). The enrichment of different REEs corresponds to different diagenetic processes. Studies of ancient cold carbonates have suggested that heavy REEs (HREEs) enrichment indicates progressive diagenetic alteration during early diagenesis in porewaters affected by a succession of biogeochemistry (Zwicker et al., 2018). In contrast, other studies on modern cold seep carbonates have shown that the enrichment of middle REEs (MREEs) and the occurrence of framboidal pyrites indicate a diagenetic environment ranging from AOM to the reduction of Fe (Crémière et al., 2016). Ce anomalies in REEs may have result from modification during late diagenesis, resulting in a negative correlation between Ce/Ce^* and Dy_N/Sm_N but a positive correlation with total REEs (∑REEs) (Shields and Stille, 2001). Some studies of ancient cold seep carbonates have found that diagenesis does not significantly alter REEs (Chen et al., 2003; Feng et al., 2009a). Therefore, the behavior of REEs in the diagenetic process of cold seep carbonates is still controversial.

In the northern Okinawa Trough, many authigenic carbonate samples related to methane seeps have been collected during various cruises (Wu et al., 2003; Sun et al., 2015). Studies have shown that different methane consumption processes occur at different sediment depths in the Okinawa Trough. Aerobic oxidation of methane is dominant in the shallow surface layer of sediments, sulfate-dependent AOM is most common in the methane-sulfate transition zone, and Fe-dependent methane consumption occurs below the methane-sulfate transition zone (Li et al., 2018). Different methane consumption processes result in different diagenetic environments. Meanwhile, some studies have found that hydrothermal activities influence cold seeps in the Okinawa Trough (Li et al., 2018; Sun et al., 2019; Wu et al., 2019). Therefore, the formation environment of cold seep carbonates in the Okinawa Trough is unique and particularly complex, and represents a unique back-arc environment where hydrothermal and cold seeps interact with each other. Thus, the effect of early diagenetic processes in such an environment must be taken into consideration. In this study, we report the

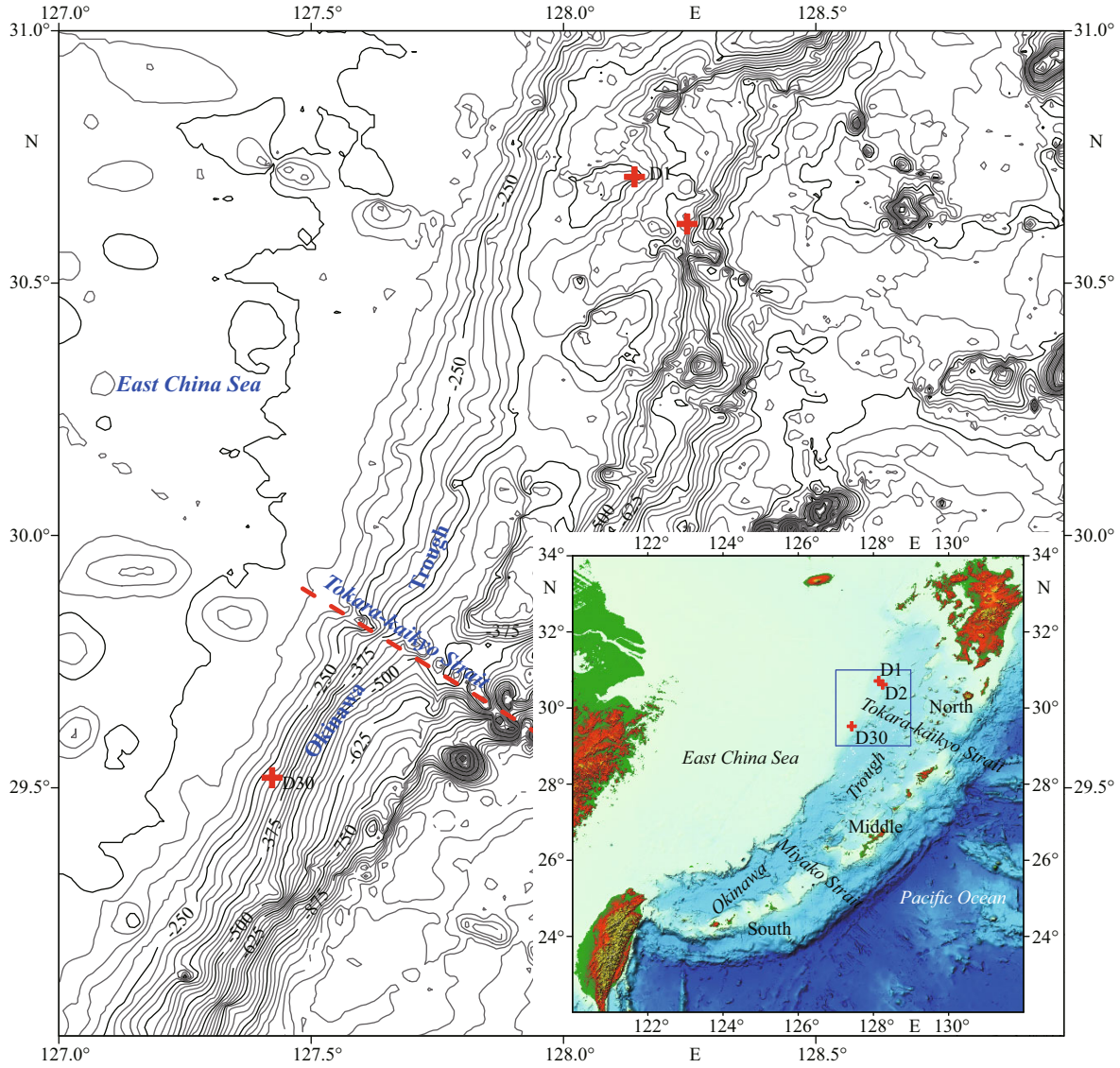

Fig.1 Locations of carbonate samples in the northern Okinawa Trough

ETOPO30″ data are used, the interval was 25 m.

mineralogy, carbon and oxygen isotopes, and REE characteristics of carbonate samples obtained in shallow water in the northern Okinawa Trough. Our aim is to study the characteristics of these carbonates and determine the corresponding implications for early diagenesis.

2 GEOLOGICAL SETTING AND SAMPLING

The Okinawa Trough, as a part of the East China Sea, is an extension bathyal basin of the trench-arc-basin tectonic system on the western Pacific continental margin (Sibuet et al., 1998). The Okinawa Trough extends approximately 1 200 km from southwest Kyushu Island (Japan) in the northeast to the Ilan Plain (Taiwan, China) in the southwest (Fig.1). Based on the submarine geomorphology and geology, the seafloor of the Okinawa Trough can be divided into three parts, namely the southern, middle, and northern sections, which are separated by the Miyako waterway and the Tokara-kaikyo strait.

The Okinawa Trough is located between the Diaoyu Islands Folded-Uplift Belt and the Ryukyu Fold-Uplifted Belt, on the west and east sides of the trough, respectively. The secondary structural units include the Shelf Front Depression, the Long Wang Uplift, and the Central Grabens, which extend along the Okinawa Trough and appear to have been cut by NW-SE faults into discontinuous arrangements, similar to en échelon veins (Liu, 1989). It has been suggested that the Okinawa Trough formed in three phases of extension beginning in the Middle to Late

Miocene, followed by reactivation in the Early Pleistocene, and concluding in the Late Pleistocene to Recent (Sibuet et al., 1998). Arc volcanism is active, and there are two modern volcanic chains, one of which is on the eastern slope, and another developed along the central fissure axis of the trough (Jin and Yu, 1987). The volcanic rocks in the Okinawa Trough are characterized by a bimodal distribution of basic basalts and acid pumice, comprising subalkaline olivine tholeiite and subalkaline (calc-alkaline) rhyolite dacite or rhyolite, respectively. The acidic pumice is the most common and is widely distributed, while the basalts are mainly exposed in the middle and southern section of the Okinawa Trough (Guo et al., 2016). Terrigenous material from the Changjiang (Yangtze) and Huanghe (Yellow) rivers is the main source of the sediments in the Okinawa Trough, although the lateral transportation of sediments from the outer shelf of the East China Sea also plays a very important role (Zhao and Wan, 2015). The high sedimentary rates and active faults on the west side supply large amounts of organic matter and providing migration channels for the formation of gas hydrates (Xu et al., 2006). Furthermore, submarine hydrothermal activities are pervasive and vigorous in the middle and southern sections of the back-arc rifts, which are principally controlled by tectonic factors (Glasby and Notsu, 2003).

Our study area is located on the western slope of the northern Okinawa Trough (Fig.1), and extends from the northern section to the northern part of the middle section. In the northern Okinawa Trough, a series of fault blocks and ridges formed in the fore slope, probably as a result of tectonic movements since the Miocene (Wu et al., 2014).

In June 2013, carbonate samples were collected by geological dredges during the survey of R/V *Kexue Yihao* (*Science No.1* in Chinese) organized by the Institute of Oceanology, Chinese Academy of Sciences. The details of the sampling sites are listed in Table 1. Four typical samples were selected for further analyses. From site D1, sample D1-1 had a homogenous structure of quartz sand with microcrystalline carbonates (Fig.2a), whereas sample D1-2 had two different structures: compacted parts and loosened parts (Fig.2b). Sample D2-1 from site D2 was compacted with some visible cracks (Fig.2c). Sample D30-1 from site D30 was compacted and contained biogenic features in the form of holes (Fig.2d).

Table 1 Locations and water depths of the carbonates collected from the northern Okinawa Trough

Site	Longitude (°E)	Latitude (°N)	Water depth (m)	Sample
D1	128.140 7	30.710 5	341.8	D1-1, D1-2
D2	128.245 0	30.617 2	561.4	D2-1
D30	127.422 6	29.520 0	255.8	D30-1

3 METHOD

The carbonate samples were air dried after collection and subsequently cut into sections for sampling and creating thin sections. The cut carbonate samples were crushed in an agate mortar to form a powder of <200 mesh, for carbon and oxygen isotope, X-ray diffraction (XRD), and REE analyses of the carbonate phases. The thin sections were observed using an optical microscope, and fresh broken rocks were examined with a Zeiss Ultra55 scanning electron microscope (SEM) at the Key Laboratory of Submarine Geosciences, Ministry of Natural Resources, China.

Carbon and oxygen isotope analyses were performed on bulk samples and were finished using a Finnigan MAT253 mass spectrometer at the State Key Laboratory of Marine Geology at Tongji University, Shanghai, China. Carbon dioxide was generated by reacting with orthophosphoric acid at 70 °C. The precision was regularly checked with an international standard (NBS19) and the standard deviation was 0.07‰ for $\delta^{18}O$ and 0.04‰ for $\delta^{13}C$. Conversion to the international Vienna Pee Dee Belemnite (V-PDB) scale was performed using the NBS19 standard.

Bulk mineralogy and the relative abundance of carbonate minerals in each sample were determined using an X'Pert Pro X-ray diffractometer with CuKα radiation at the Key Laboratory of Submarine Geosciences, Ministry of Natural Resources. Oriented samples were scanned at an interval of 3°–70° (2θ) with a step size of 0.017°, an accelerating voltage of 45 kv, and a current of 40 mA. Semi-quantitative phase analyses were performed using the MDI Jade 6.0 software. The relative proportions of different carbonate minerals were quantified using calibration curves according to the d(104) peak areas of calcite, Mg-calcite, and dolomite, and the d(111) peak area of aragonite (Greinert et al., 2001). The molar $MgCO_3$ percentage of calcite was calculated using the d(104) peak value of calcite (in Å), following the equation by Lumsden (1979):

$$MgCO_3\,(\%\text{ in mole fraction, hereafter abbreviated as mol\%}) = 100 - (333.33 \cdot d(104) - 911.99), \quad (3)$$

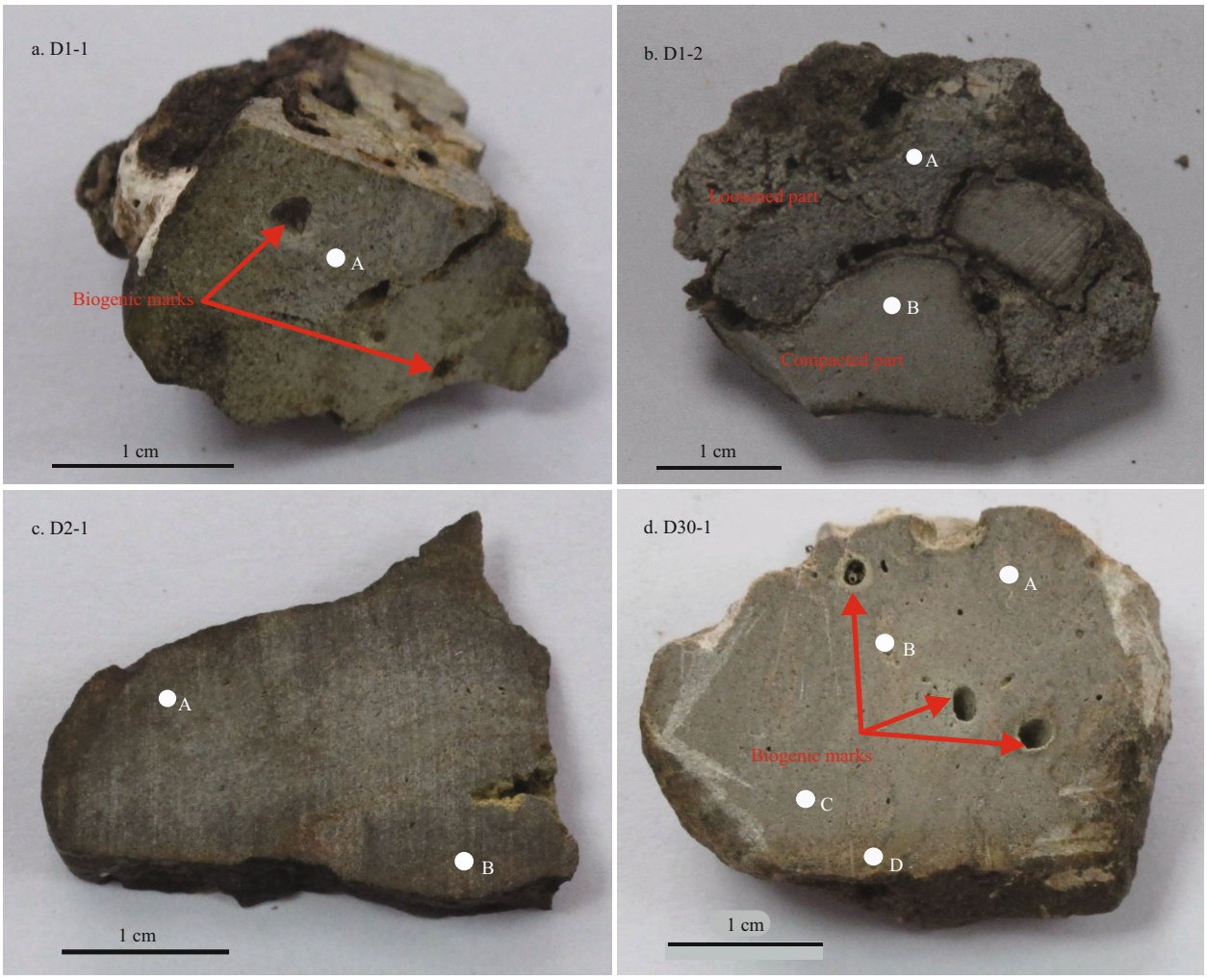

Fig.2 Photographs of the carbonate samples collected from the northern Okinawa Trough

The white points and labels indicate the sampling locations for carbon and oxygen isotope analyses.

where *d*(104) is the *d*(104) peak value of calcite (in Å).

Calcite containing less than 5 mol% $MgCO_3$ was considered to be LMC, and calcite containing 5–20 mol% $MgCO_3$ was referred to as HMC (Burton, 1993). Carbonate phases with 30–40 mol% $MgCO_3$ were classified as proto-dolomite, and carbonates containing 40–55 mol% $MgCO_3$ are referred to as dolomite (Naehr et al., 2007). The dolomite in this study includes both proto-dolomite and ordered dolomite.

The REEs of carbonate phases were determined at the Guizhou Tuopujing Resource and Environmental Analysis Co., Ltd. About 50 mg of powdered sample were placed in a 50-mL centrifuge tube, about 40-mL water and 500-ng Rh internal standard were added, and then 2.5 mL of acetic acid (98%, purified by sub-boiling) was added to dissolve the carbonate. The sealed tube was vibrated for about 1 h and then centrifuged for 3 min at 3 000 r/min. The upper solution was used to measure the REEs by inductively coupled plasma mass spectrometry (ICP-MS). The accuracies were estimated to be better than ±5%–10% (relative) for most elements. In this study, $Ce/Ce^{*}=3Ce_N/(2La_N+Nd_N)$, $Ce_{anom}=\log(Ce/Ce^{*})$, $Eu/Eu^{*}=2Eu_N/(Sm_N+Gd_N)$, and $Pr/Pr^{*}=2Pr_N/(Ce_N+Nd_N)$, where N refers to the normalization of the concentration against the standard Post-Archean Australian Shale (PAAS; McLennan, 1989).

The total carbonate content (%) was estimated from the soluble percentage of the bulk samples, analyzed for REE composition of carbonate phases, after acetic acid was added to dissolve the carbonate completely (for detailed procedures see the method for REEs analysis mentioned above). The weight of the residue after freeze-drying was used to calculate the carbonate content as follow:

$$\text{Carbonate content}=(50-\text{residue weight})/50\times100\%. \quad (4)$$

The resulting accuracies were better than ±2%.

Table 2 Mineralogical compositions of carbonates from the northern Okinawa Trough

Sample	Q	Ab	Clc	Mc	Ms	Ara	LMC		HMC		Dol		∑carb[a]	∑carb[b]
	(%)						(%)	Mg%	(%)	Mg%	(%)	Mg%	(%)	
D1-1	39	11	7	6	5	24	5	1	–	–	3	49	32	31.8
D1-2LP	39	9	2	3	2	41	3	2	–	–	1	50	45	47.3
D1-2CP	21	8	5	6	10	1	–	–	43	17	6	38	50	54.9
D2-1	31	8	7	8	9	–	4	1	–	–	33	43	37	40.8
D30-1	34	13	5	4	4	–	–	–	32	19	7	34	41	45.8

D1-2LP: the loosened parts of sample D1-2; D1-2CP: the compacted parts of sample D1-2; Q: quartz; Ab: albite; Clc: clinochlore; Mc: microcline; Ms: mica; Ara: aragonite; LMC: low-Mg calcite; HMC: high-Mg calcite; Dol: dolomite; ∑carb[a]: the calculation results based on the semi-quantitative XRD; ∑carb[b]: the calculation results according to the soluble percentage of the REE analysis samples after the acetic acid was added to dissolve the carbonates completely. %: weight percent; Mg%: mole percent of $MgCO_3$ in carbonate minerals. – means no such mineral was found.

4 RESULT

4.1 Mineralogy and petrology

The semi-quantitative XRD results are listed in Table 2. In general, for all the studied samples, the main carbonate phases were aragonite, HMC, and dolomite; however, the main carbonate minerals varied among the samples. For example, in sample D1-2, aragonite was the main carbonate mineral in the loosened parts, but HMC was more predominant in the compacted parts. The LMC content was low in all the samples in which it was detected. The total carbonate content of bulk rocks varied from 32% to 50% based on the semi-quantitative XRD analysis, and from 31.8% to 54.9% based on the soluble percentage of the REE analysis of carbonate phases (Table 2).

The macroscopic characteristics of the authigenic carbonate samples are shown in Fig.3. All the samples had microcrystalline structures (Fig.3a), except the compacted parts of sample D1-2, which exhibited a cryptocrystal structure (Fig.3b). Framboidal pyrites, which ranged in diameter with individual grains of 1–2 μm, were found in sample D30-1 (Fig.3c). Most framboids were oxidized to goethite or limonite (details see Yang et al., 2021). Pyrites were also found in sample D2-1, but they occurred as aggregates or single euhedral crystals with brown rims of goethite or limonite (Fig.3d).

All the samples were observed under SEM, and some interesting phenomena are shown in Fig.4. Aragonite in sample D1-1 and the loosened parts of D1-2 comprised acicular crystals of approximately 100 μm in length (Fig.4a). The HMC minerals occurred as rice-shaped crystals (Fig.4b). Different types of microbial structures were observed. Carbonate minerals were joined to the ambient environment by filaments (Fig.4c). Flat filaments with segments forming mats were observed to be twisted, and each segment was approximately 0.3–0.5 μm in diameter and 1–1.5 μm in length, implying that the new filaments sprouted from the joints of older segments (Fig.4d & e). Numerous biological tests were identified, such as siliceous sponge spicules and coccoliths (Fig.4f & g).

4.2 Carbon and oxygen isotopes

The carbonate minerals exhibited microcrystalline or cryptocrystal textures; thus, carbon and oxygen isotope analyses were performed on the bulk rocks. The sampled locations for the carbon and oxygen isotope analyses are labeled in Fig.2, and the $\delta^{13}C$ and $\delta^{18}O$ values of all the carbonate samples are listed in Table 3. The $\delta^{13}C$ values of carbonates from the northern Okinawa Trough varied from -53.7‰ to -39.3‰, with an average of -47.3‰ (V-PDB, n=9). The $\delta^{18}O$ values ranged from 0.6‰ to 3.4‰, with an average of 1.9‰ (V-PDB, n=9).

4.3 Rare earth element analysis

The REE data of the carbonate phases from the northern Okinawa Trough are presented in Table 4 and Fig.5. The ∑REE content of the studied carbonates ranged from 12.86×10^{-6} to 28.76×10^{-6}. No samples showed any Ce anomalies; all of the Ce/Ce^{*} values were between 0.8 and 1.2, whereby values of <0.8 indicate negative Ce anomalies, and values of >1.2 indicate positive Ce anomalies. All samples were slightly enriched in MREEs.

5 DISCUSSION

5.1 Diagenetic fluids traced with C and O isotopes

Stable carbon isotopes of authigenic carbonates are critical to deciphering the source of seepage fluids (e.g., Campbell, 2006). Such fluids likely originate

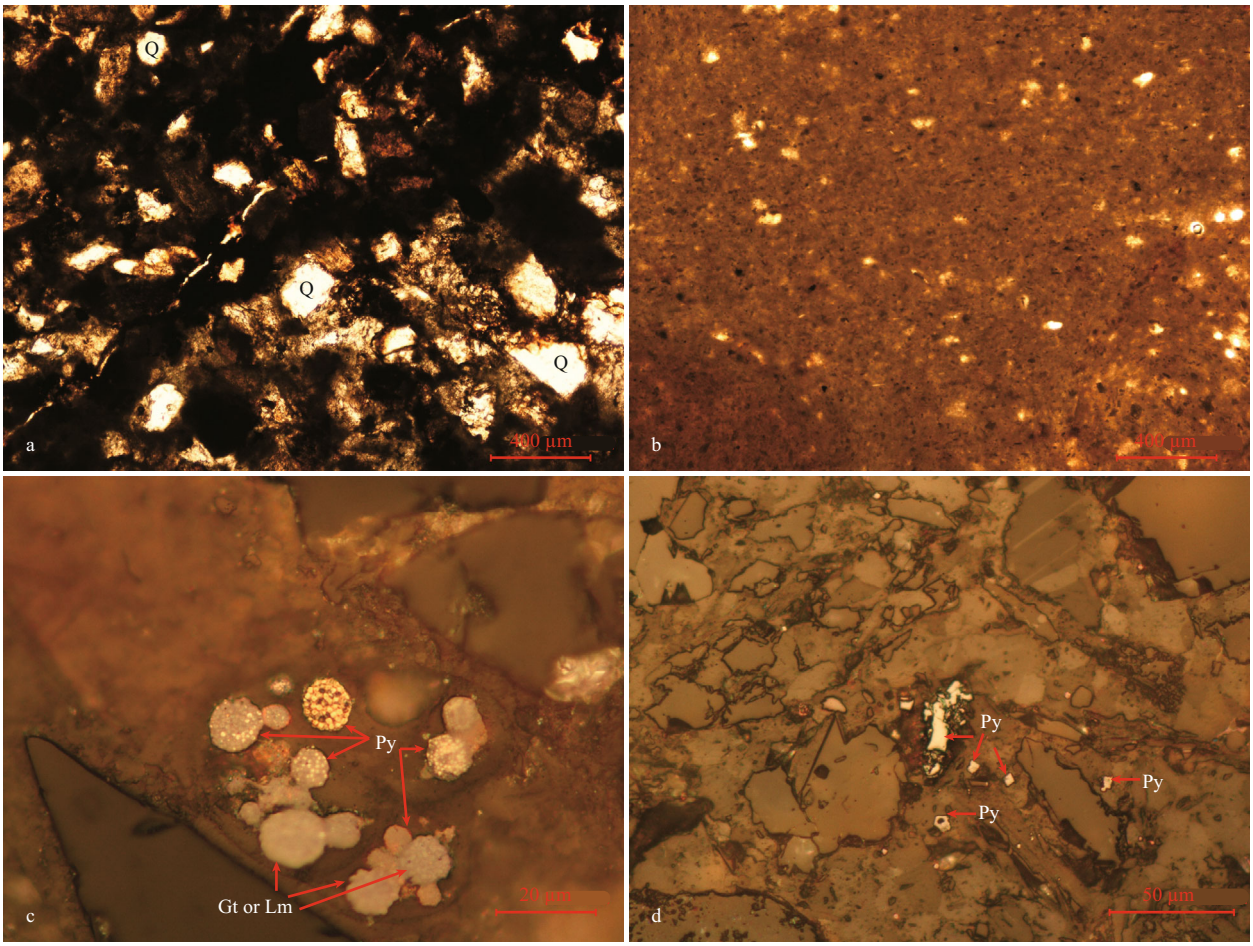

Fig.3 Thin section photographs of carbonate samples

a–b. taken under plane polarized light; c–d. taken under reflected light. a. the loosened parts of sample D1-2, showing microcrystalline structure; b. the compacted parts of sample D1-2, showing cryptocrystal structure; c. framboidal pyrites filling the interior of a foraminifera test (some have been oxidized to brown goethite or limonite) in sample D30-1; d. pyrites with brown goethite or limonite rims in sample D2-1; Q: quartz; Py: pyrite; Gt: goethite; Lm: limonite.

Table 3 Stable carbon and oxygen isotopic compositions of the carbonates from the northern Okinawa Trough (‰, V-PDB)

Sample	Location	$\delta^{13}C$	$\delta^{18}O$	Description
D1-1	A	-47.0	0.6	The structure is homogeneous, so sampled randomly
D1-2LP	A	-46.7	0.9	In the loosened parts
D1-2CP	B	-36.2	1.7	In the compacted parts
D2-1	A	-43.9	1.4	In the cyan color place
D2-1	B	-39.3	1.9	In the brown color place
D30-1	A	-53.7	2.3	In the greyish white place
D30-1	B	-53.1	2.4	In the loose greyish white place
D30-1	C	-53.6	3.4	In the cyan color place
D30-1	D	-52.6	2.6	In the brown color place

The sampled locations are labeled in Fig.2, and the data of sample D30-1 are from Yang et al. (2021).

from a mixture of sources with varying proportions, resulting in distinct carbon isotopic compositions (Mazzini et al., 2004). These sources comprise carbon primarily derived from: 1) methane via AOM (typically ranging between -90‰ and -30‰) (Claypool and Kaplan, 1974); 2) the oxidation of marine organic matter (usually ≅ -20‰); 3) inorganic carbon present in seawater (0.5‰< $\delta^{13}C$ <2‰) (e.g., Irwin et al., 1977). Seep carbonates are frequently characterized by extremely light carbon isotopic compositions (e.g., Suess, 2014, and references therein). A strong depletion of ^{13}C in carbonates ($\delta^{13}C$ values between -50‰ and -25‰) is evidence of a methane-related origin (Cavagna et al., 1999). The $\delta^{13}C$ values of the carbonate samples from the northern Okinawa Trough varied from -53.7‰ to -39.3‰; thus, we speculate the main carbon source was derived from methane via AOM.

Methane can be derived from biogenic methane, thermogenic methane, or petroleum. The carbon isotope composition of biogenic methane is strongly depleted in ^{13}C, varying from -110‰ to -50‰

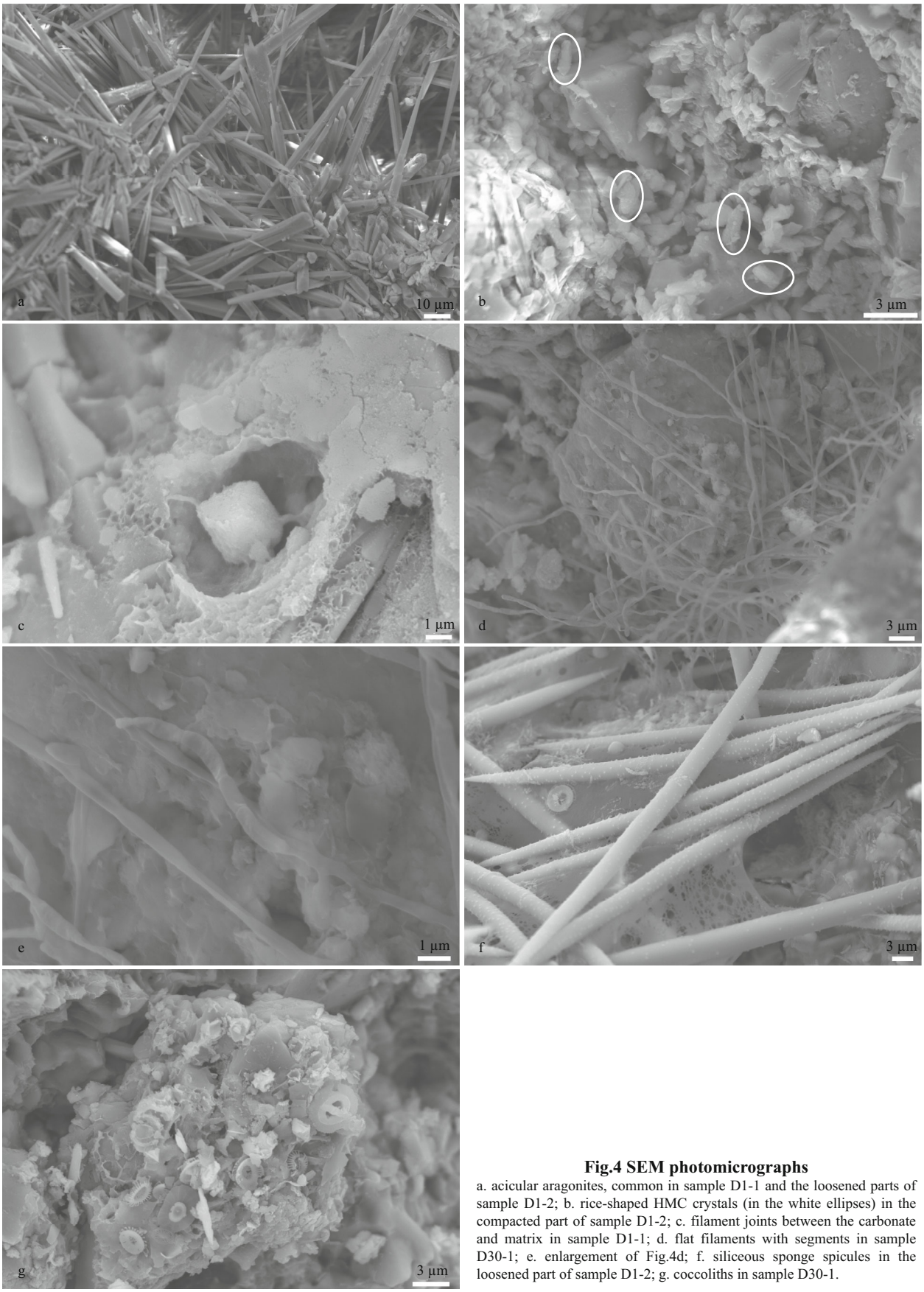

Fig.4 SEM photomicrographs

a. acicular aragonites, common in sample D1-1 and the loosened parts of sample D1-2; b. rice-shaped HMC crystals (in the white ellipses) in the compacted part of sample D1-2; c. filament joints between the carbonate and matrix in sample D1-1; d. flat filaments with segments in sample D30-1; e. enlargement of Fig.4d; f. siliceous sponge spicules in the loosened part of sample D1-2; g. coccoliths in sample D30-1.

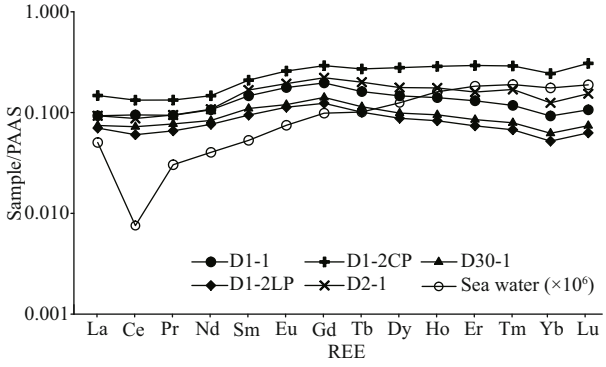

Fig.5 The PASS-normalized REE patterns of authigenic carbonates

D1-2LP: the loosened parts of sample D1-2; D1-2CP: the compacted parts of sample D1-2. Seawater data represents the average values above a depth of 600 m from Alibo and Nozaki (1999) which are consistent with the water depths of the carbonate samples.

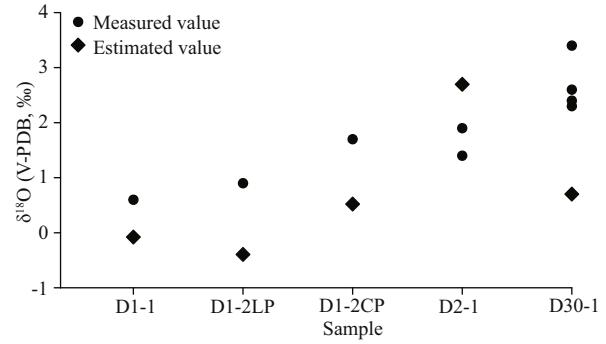

Fig.6 Comparison of $\delta^{18}O$ values between the measured and estimated values

(Whiticar, 1999). The carbon isotope composition of thermogenic methane typically ranges from -50‰ to -30‰ (Sackett, 1978), while that of petroleum usually exhibits $\delta^{13}C$ values in the range of -35‰ to -25‰ (Roberts and Aharon, 1994). Because carbonate precipitates also contain other sources of carbon that usually have a higher ^{13}C content, the $\delta^{13}C$ value of seep carbonates will generally be higher than that of seeping methane. The $\delta^{13}C$ values of the carbonate samples from the northern Okinawa Trough varied from -53.7‰ to -39.3‰, with an average of -47.3‰, which is between the values of thermogenic and biogenic methane, but much closer to the thermogenic endmember (Sackett, 1978; Whiticar, 1999). Therefore, we propose that the carbon in the seep carbonates was derived from a mix of thermogenic methane and biogenic methane, with perhaps a greater contribution from the former.

The oxygen isotope composition of authigenic carbonates is a function of temperature and mineralogy, which affect oxygen isotope fractionation and the $\delta^{18}O$ value of the fluid (Aloisi et al., 2000).

Table 4 The rare earth elements contents ($\times10^{-6}$) of authigenic carbonate phases in carbonate rocks

Sample	D1-1	D1-2LP	D1-2CP	D2-1	D30-1
La	3.55	2.68	5.64	3.55	2.84
Ce	7.55	4.80	10.58	6.95	5.76
Pr	0.83	0.58	1.18	0.84	0.68
Nd	3.61	2.59	4.98	3.66	2.83
Sm	0.81	0.52	1.16	0.93	0.61
Eu	0.19	0.12	0.28	0.21	0.13
Gd	0.92	0.58	1.36	1.03	0.66
Tb	0.13	0.08	0.21	0.15	0.09
Dy	0.68	0.41	1.31	0.83	0.46
Ho	0.14	0.08	0.29	0.17	0.09
Er	0.37	0.21	0.84	0.46	0.24
Tm	0.05	0.03	0.12	0.07	0.03
Yb	0.26	0.15	0.69	0.35	0.18
Lu	0.05	0.03	0.13	0.07	0.03
∑REE	19.14	12.86	28.76	19.27	14.65
Ce/Ce*	0.97	0.84	0.90	0.89	0.93
Ce_{anom}	-0.01	-0.08	-0.04	-0.05	-0.03
Eu/Eu*	1.03	1.04	1.03	1.00	0.95
Pr/Pr*	0.93	0.96	0.95	0.97	0.99
La_N/Sm_N	0.63	0.74	0.71	0.56	0.68

D1-2LP: the loosened parts of sample D1-2; D1-2CP: the compacted parts of sample D1-2.

According to Sun et al. (2015), the theoretical $\delta^{18}O$ values for carbonate precipitates in our study area are -0.52‰, 0.2‰, and 3.00‰ (V-PDB) for calcite, aragonite, and dolomite, respectively. Because all the samples contained more than one carbonate mineral, we hypothesize that the oxygen isotope fractionation was at equilibrium for each carbonate mineral (Aloisi et al., 2000). Accordingly, the estimated $\delta^{18}O$ values calculated for each sample are shown in Fig.6. The values were estimated as follows:

$$^{18}O_{estimated}\,(‰) = -0.52‰ \times \text{calcite relative ratio} + 0.2‰ \times \text{aragonite relative ratio} + 3.00‰ \times \text{dolomite relative ratio},$$

where calcite relative ratio=calcite content/(calcite content+aragonite content+dolomite content), and so on.

All the measured $\delta^{18}O$ values were higher than the estimated values, except for sample D2-1, which had a maximum difference of 2.7‰ (Fig.6). Thus, there must have been some $\delta^{18}O$-enriched fluids involved in the process of carbonate precipitation. Both clay mineral dehydration and gas hydrate dissociation can

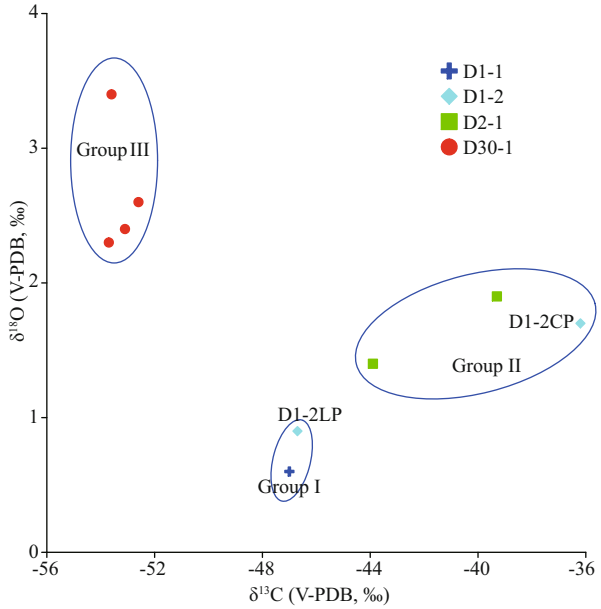

Fig.7 Samples grouped according to carbon and oxygen isotopes, indicating their different formation environments

Group I indicates a coarse-grained environment; Group II indicates a fine-grained environment; and Group III indicates a fine-grained environment with common biological activities.

result in ^{18}O-enriched fluids (e.g., Sun et al., 2015; Cao et al., 2020). Carbonate precipitation mediated by AOM always occurs in shallow sediments, while the dehydration of clay minerals occurs at greater depths (>1 km) (e.g., Sun et al., 2015; Cao et al., 2020). In addition, no volcanoes or mud diapirs have been reported in the study area. Therefore, the ^{18}O-enriched fluid cannot possibly have been caused by clay mineral dehydration, which leaves gas hydrate dissociation as the most likely explanation. Moreover, there are favorable geological conditions for the formation of gas hydrate in the study area, and the bottom simulating reflectors (BSRs) indicating the existence of gas hydrate were also found (e.g., Luan et al., 2008). However, the measured ^{18}O value of sample D2-1 was lower than the estimated value. The main carbonate mineral of sample D2-1 was dolomite, which could be the result of diagenesis (Frisia et al., 2018). Diagenesis more commonly causes $\delta^{18}O$ to become more negative (Swart, 2015); thus, we hypothesize that the measured ^{18}O value was lower than the estimated value due to diagenesis. The original $\delta^{18}O$ value of sample D2-1 should have been higher than the measured value, and it may have been higher than the estimated value when it originally precipitated. Therefore, ^{18}O-enriched fluid also played a role in the precipitation of sample D2-1.

According to the characteristics of the measured carbon and oxygen isotopes, the samples were roughly classified into three groups: low ^{13}C with high ^{18}O, moderate ^{13}C with low ^{18}O, and high ^{13}C with moderate ^{18}O (Fig.7), indicating the different environments in which they formed. Based on the carbon and oxygen isotope data, the loosened and compacted parts of sample D2-1 belonged to different groups, suggesting that environmental change occurred during its precipitation (see Section 5.2).

5.2 Petrological and mineralogical characteristics and their implications

5.2.1 Structural characteristics and their implication for formation processes

After the precipitation of carbonate minerals, a series of physical, chemical, and biological processes can change the composition, geochemistry, and structure of cold seep carbonates (Morse, 2003).

According to macroscopic observations, the sediments cemented by carbonate minerals in this study could be divided into two types: fine grained and coarse grained. Sample D1-1 and the loosened parts of sample D1-2 were composed of relatively coarse-grained sediments. Samples D2-1 and D30-1 and the compacted part of sample D1-2 comprised fine-grained sediments. In particular, sample D1-2 exhibited two completely different structures: a fine-grained structure (the compacted parts) and a coarse-grained structure (the loosened parts). The different grain sizes of cemented sediments were more obvious under a polarizing microscope (Fig.3a & b). In addition, the main carbonate minerals, the C and O isotopes, and the ∑REE content of the different groups were clearly different (Tables 2–4). Therefore, we infer the existence of at least two different diagenetic environments, based on the carbonate structures.

There are two possible explanations for the obvious structural difference within sample D1-2. Either sediments with different grain sizes were deposited in different sedimentary environments and then mixed by bioturbation or slides (e.g., Luff et al., 2004; Panieri et al., 2012) before being cemented by methane-related carbonate minerals, or there were different periods of methane seepage, and the existing cemented carbonates were recemented during the formation of the later methane-related carbonates. If the first explanation is correct, the minerals, isotopes, and the ∑REE content would be similar across the different structures; however, these characteristics exhibited obvious differences (Tables 2–4). This was

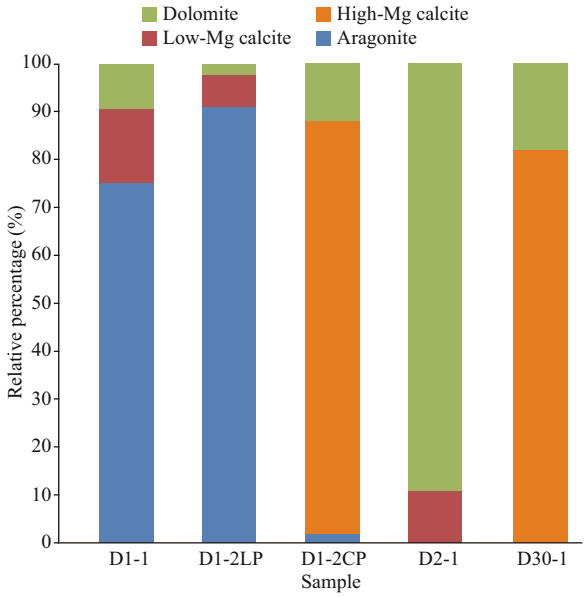

Fig.8 Relative percentages of carbonate minerals among samples

especially true for the minerals: the loosened parts were mainly composed of aragonite, while the compacted parts contained mostly HMC. It is commonly accepted that in cold seep environments, aragonite forms under relatively high SO_4^{2-} and low PO_4^{3-} concentrations, whereas Mg-calcite precipitation is favored under relatively high PO_4^{3-} and low SO_4^{2-} solutions (Greinert et al., 2001; Peckmann et al., 2001). Some studies have reported that aragonite is precipitated during periods of high methane seep activity whereas HMC forms during periods of low methane seepage (Nöthen and Kasten, 2011; Pierre et al., 2012). As such, aragonite is preferentially formed in more open systems such as sedimentary environments close to the seafloor (Magalhães et al., 2012). Therefore, we speculate that the compacted parts of sample D1-2 formed in deeper sediments, containing solutions with relatively low SO_4^{2-} concentrations, and were then moved up to a shallow depth (even to the seafloor) by subsequent uplift and erosion (Peng et al., 2017). Subsequently, the loosened parts cemented with the former compacted parts during the later methane seepage periods. Thus, the different structures of sample D1-2 relate to different periods of methane seepage, which are common in cold seeps (e.g., Liebetrau et al., 2010; Feng and Chen, 2015; Franchi et al., 2017). Multistage methane seepages have been documented in the study area (Cao et al., 2020). However, we did not observe any evidence of dissolution and recrystallization of carbonate minerals under the polar microscope, possibly because the carbonate minerals were cryptocrystalline or microcrystalline.

Biogenic structures were also observed in the carbonate samples, for instance, D1-1 and D30-1 contained obvious biogenic holes (Fig.2a & d). SEM observations revealed rice-shaped and flat filamentous microbial structures (Fig.4b, d, & e). Such structures have also been recorded in methane-related carbonate samples from other sites, such as the South China Sea (Han et al., 2008), the northern-central Adriatic Sea (Capozzi et al., 2012), and the Sea of Marmara (Turkey) (Crémière et al., 2012). The rice-shaped microbial structures were interpreted as calcified sulfate-reducing bacteria cells (Capozzi et al., 2012). A mineralized microbe-like tubular structure was also observed in another study in the Okinawa Trough (Cao et al., 2020). Therefore, biological and microbial activities are actively involved in the formation of cold seep carbonates in the Okinawa Trough.

5.2.2 Mineral characteristics and their implications

The composition of carbonate minerals reflects their precipitation environment (Naehr et al., 2007; Pierre et al., 2012, and references therein); therefore, they can be used to trace the formation environment of carbonates. The carbonate minerals of each sample differed, but each sample had one dominant carbonate mineral (Table 2; Fig.8). In particular, sample D1-2 comprised different structures with different dominant carbonate minerals. The main carbonate minerals of the samples were all aragonite or HMC, except for sample D2-1 in which the main carbonate mineral was dolomite.

The formation environment of aragonite and HMC was described in Section 5.2.1. Some studies have shown that dolomite precipitation can occur under relatively low dissolved SO_4^{2-} concentrations (Baker and Kastner, 1981). The experimental study of Warthmann et al. (2000) demonstrated that sulfate-reducing bacteria could influence dolomite precipitation under controlled low-temperature anoxic conditions. The experiment calculation showed that AOM increases the CO_3^{2-} concentration through sulfate reduction, thus favoring dolomite formation (Moore et al., 2004). Dolomite can form because of diagenesis (Frisia et al., 2018). Therefore, sample D2-1 may have been formed at great depth, where the SO_4^{2-} concentration was low and/or diagenesis occurred. The results of oxygen isotope analysis suggest that early diagenesis probably played a major role in the precipitation of sample D2-1. In all

the samples, HMC or dolomite was the main carbonate mineral in the fine grained structure (Fig.7, Groups II and III), while aragonite was the main carbonate mineral in the coarse grained structure (Fig.7, Group I). This shows that the different structures could be differentiated by their carbonate mineral compositions.

Authigenic pyrite is a common mineral in cold seep carbonates, and forms from the HS^- generated by sulfate-dependent AOM and free Fe^{2+} in porewaters (Fan et al., 2018). Pyrite associated with cold seeps has various morphologies, but the main morphology is framboidal (e.g., Chen et al., 2006; Lin et al., 2016; Pierre, 2017). In sample D30-1, many framboidal pyrites were observed in calcareous tests, and are assumed to be related to methane seepage. However, in sample D2-1, pyrite occurred as aggregates or euhedral crystals without the rounding marks of having undergone long-distance transport. These crystals were thought to be related to the nearby hydrothermal sources, which have been verified as influencing carbonate formation in the studied area (Li et al., 2018; Sun et al., 2019; Wu et al., 2019). However, because pyrites with different genetic types were all oxidized to iron oxides or hydroxides, we assume that they were all influenced by early diagenesis.

The total carbonate mineral content of the carbonate samples was not high and was even <50% in coarse grained structures with relatively high porosity (Table 2). The precipitation of carbonate minerals can be affected by the methane seepage rate and porosity (Luff et al., 2004). Therefore, the relatively low carbonate mineral contents of our samples are attributable to the methane flux rate.

5.3 REEs and their implications

The REE pattern of marine carbonates can be used as a geochemical proxy for the reconstruction of fluid composition and physicochemical variations (Franchi et al., 2017). Among the REEs, Ce and Eu are very sensitive to redox reactions. However, as our results showed no Ce and Eu anomalies, they do not agree with findings for samples from the South China Sea (e.g., Wang et al., 2014) and other sites (e.g., Rongemaille et al., 2011; Feng et al., 2013). Previous studies have demonstrated that the proxy log(Ce/Ce*) (labeled Ce_{anom}) can be used to trace precipitation environments when REEs are shale-normalized (e.g., Feng et al., 2009b). A Ce_{anom} value of >-0.1, indicates anoxic conditions, whereas a Ce_{anom} value of <-0.1 indicates oxic conditions (Wright et al., 1987). The Ce_{anom} values of our samples were all >-0.1 (Table 4), suggesting that they all precipitated in an anoxic environment. Pyrite framboids were observed in some samples, confirming that anoxic conditions prevailed during carbonate precipitation.

Another obvious characteristic of the REEs in the carbonate samples from the northern Okinawa Trough was a slight enrichment of MREEs, which was consistent with findings for other sites, such as the Makran accretionary prism and the Gulf of Mexico (Feng et al., 2009a; Himmler et al., 2013). Iron and manganese oxides preferentially adsorb MREEs, which can create a MREE bulge pattern (Bayon et al., 2011; Rongemaille et al., 2011). Organic matter may be an additional source of MREEs (Freslon et al., 2014). Some enrichment of MREEs is due to diagenetic overprinting (Shields and Stille, 2001). If the La_N/Sm_N ratio is >0.35 and it is not correlated with the Ce anomaly (Ce/Ce*), late diagenesis had no effect on REEs (Wang et al., 2014). All the La_N/Sm_N values of our samples were >0.35 (Table 4), and the samples did not show any correlation between La_N/Sm_N and Ce/Ce* ratios. However, the oxygen isotopes and mineral characteristics implied that sample D2-1 was affected by early diagenesis. When sample D2-1 was excluded, the La_N/Sm_N and Ce/Ce* ratios of the samples did exhibit a strong negative relationship (R^2=0.972), indicating the influence of early diagenesis on samples D1-1, D1-2, and D30-1.

Some previous studies have suggested that the REE compositions of cold seep carbonates are primarily controlled by the REE compositions of carbonate minerals and the fluids from which they were precipitated (Rongemaille et al., 2011). The REE patterns can be used to reconstruct ancient environmental conditions during the seep carbonates formation, and can provide insight into changes in seawater and sedimentary pore water compositions as well as diagenetic alteration during early diagenesis in marine pore waters, which is affected by a succession of biogeochemical reactions (Zwicker et al., 2018). For carbonates precipitating from seawater, any deviation from the REE distribution of seawater can be regarded as being of diagenetic origin (Smrzka et al., 2020). In modern cold seeps, aragonite forms close to the sediment-water interface, in pore waters with a very similar composition to that of seawater (Zwicker et al., 2018). Therefore, its REE pattern should be similar to that of seawater. The main carbonate mineral of Sample D1-1 and D2-1LP is aragonite, however their normalized REE patterns

displayed a non-marine seawater trend (Fig.5), which indicated that some diagenetic influences have masked the seawater signature. Some studies have indicated that different carbonate minerals, even the different crystal forms of the same carbonate mineral, can exhibit different REE patterns (Himmler et al., 2010; Franchi et al., 2017; Zwicker et al., 2018). However, all the studied samples exhibited a similar REE pattern; even they contained different carbonate minerals. Therefore, the REE compositions of the samples in our study are not indicative of the compositions of the ambient fluids from which they originally precipitated. Some influences, most likely early diagenesis, have masked the REE pattern of the original pore waters.

6 CONCLUSION

The authigenic carbonate samples collected from the northern Okinawa Trough formed because of AOM in methane seepages. The dominant carbonate minerals in different samples indicated the environment and process of carbonate precipitation. Multistage methane seepages were inferred to have formed these samples, based on structural, mineralogical, and petrological observations. The $\delta^{13}C$ values of carbonate samples from the northern Okinawa Trough varied from -53.7‰ to -39.3‰, with an average of -47.3‰, suggesting that the main carbon source was a mixture of thermogenic methane and biogenic methane, possibly with a greater contribution from the former. The $\delta^{18}O$ values ranged from 0.6‰ to 3.4‰, with an average of 1.9‰ indicating that the ^{18}O-enriched fluids from gas hydrate dissociation took part in the carbonate precipitation process. The REE results revealed an enrichment of MREEs but no Ce anomalies, and the Ce_{anom} values suggested that all the carbonate samples might have precipitated in an anoxic environment, which was confirmed by the occurrence of pyrite framboids. Structural, mineral, oxygen isotope, and MREE data collectively implied that the carbonates from the northern Okinawa Trough underwent early diagenesis.

7 DATA AVAILABILITY STATEMENT

All data generated and/or analyzed during this study are included in this published article.

8 ACKNOWLEDGMENT

We are grateful to the crew and scientists on R/V *Kexue Yihao* for collecting samples during the expedition in June 2013, which was organized by the Institute of Oceanology, Chinese Academy of Sciences (CAS). We thank Dr. Xiaoying JIANG at Tongji University for analyzing the carbon and oxygen isotopes, Dr. Liang QI at the Institute of Geochemistry, CAS, for analyzing the REEs, and Dr. Jihao ZHU at the Key Laboratory of Submarine Geosciences, Ministry of Natural Resources for his help in the SEM analysis. We thank the two anonymous reviewers for their constructive comments, which helped to considerably improve the manuscript.

References

Alibo D S, Nozaki Y. 1999. Rare earth elements in seawater: particle association, shale-normalization, and Ce oxidation. *Geochimica et Cosmochimica Acta*, **63**(3-4): 363-372.

Aloisi G, Pierre C, Rouchy J M, Foucher J P, Woodside J, the MEDINAUT Scientific Party. 2000. Methane-related authigenic carbonates of eastern Mediterranean Sea mud volcanoes and their possible relation to gas hydrate destabilisation. *Earth and Planetary Science Letters*, **184**(1): 321-338.

Baker P A, Kastner M. 1981. Constraints on the formation of sedimentary dolomite. *Science*, **213**(4504): 214-216.

Bayon G, Birot D, Ruffine L, Caprais J C, Ponzevera E, Bollinger C, Donval J P, Charlou J L, Voisset M, Grimaud S. 2011. Evidence for intense REE scavenging at cold seeps from the Niger Delta margin. *Earth and Planetary Science Letters*, **312**(3-4): 443-452.

Boetius A, Ravenschlag K, Schubert C J, Rickert D, Widdel F, Gieseke A, Amann R, Jørgensen B B, Witte U, Pfannkuche O. 2000. A marine microbial consortium apparently mediating anaerobic oxidation of methane. *Nature*, **407**(6804): 623-626.

Burton E A. 1993. Controls on marine carbonate cement mineralogy: review and reassessment. *Chemical Geology*, **105**(1-3): 163-179.

Campbell K A. 2006. Hydrocarbon seep and hydrothermal vent paleoenvironments and paleontology: past developments and future research directions. *Palaeogeography, Palaeoclimatology, Palaeoecology*, **232**(2-4): 362-407.

Cao H, Sun Z L, Wu N Y, Liu W L, Liu C L, Jiang Z K, Geng W, Zhang X L, Wang L B, Zhai B, Jiang X J, Liu L P, Li X. 2020. Mineralogical and geochemical records of seafloor cold seepage history in the northern Okinawa Trough, East China Sea. *Deep Sea Research Part I: Oceanographic Research Papers*, **155**: 103165.

Capozzi R, Guido F L, Oppo D, Gabbianelli G. 2012. Methane-derived Authigenic carbonates (MDAC) in northern-central Adriatic Sea: relationships between reservoir and methane seepages. *Marine Geology*, **332-334**: 174-188.

Cavagna S, Clari P, Martire L. 1999. The role of bacteria in the formation of cold seep carbonates: geological evidence

from Monferrato (Tertiary, NW Italy). *Sedimentary Geology*, **126**(1-4): 253-270.

Chen D F, Dong W Q, Qi L, Chen G Q, Chen X P. 2003. Possible REE constraints on the depositional and diagenetic environment of Doushantuo Formation phosphorites containing the earliest metazoan fauna. *Chemical Geology*, **201**(1-2): 103-118.

Chen D F, Feng D, Su Z, Song Z G, Chen G Q, Cathles III L M. 2006. Pyrite crystallization in seep carbonates at gas vent and hydrate site. *Materials Science and Engineering*: *C*, **26**(4): 602-605.

Claypool G E, Kaplan I R. 1974. The origin and distribution of methane in marine sediments. *In*: Kaplan I R ed. Natural Gases in Marine Sediments. Springer, Boston. p.99-139.

Crémière A, Lepland A, Chand S, Sahy D, Kirsimäe K, Bau M, Whitehouse M J, Noble S R, Martma T, Thorsnes T, Brunstad H. 2016. Fluid source and methane-related diagenetic processes recorded in cold seep carbonates from the Alvheim channel, central North Sea. *Chemical Geology*, **432**: 16-33.

Crémière A, Pierre C, Blanc-Valleron M, Zitter T, Çağatay M N, Henry P. 2012. Methane-derived authigenic carbonates along the North Anatolian fault system in the Sea of Marmara (Turkey). *Deep Sea Research Part I*: *Oceanographic Research Papers*, **66**: 114-130.

Fan L F, Lin S, Hsu C W, Tseng Y T, Yang T F, Huang K M. 2018. Formation and preservation of authigenic pyrite in the methane dominated environment. *Deep Sea Research Part I*: *Oceanographic Research Papers*, **138**: 60-71.

Feng D, Chen D F, Peckmann J. 2009a. Rare earth elements in seep carbonates as tracers of variable redox conditions at ancient hydrocarbon seeps. *Terra Nova*, **21**(1): 49-56.

Feng D, Chen D F, Roberts H H. 2009b. Petrographic and geochemical characterization of seep carbonate from Bush Hill (GC 185) gas vent and hydrate site of the Gulf of Mexico. *Marine and Petroleum Geology*, **26**(7): 1190-1198.

Feng D, Chen D F. 2015. Authigenic carbonates from an active cold seep of the northern South China Sea: new insights into fluid sources and past seepage activity. *Deep Sea Research Part II*: *Topical Studies in Oceanography*, **122**: 74-83.

Feng D, Lin Z J, Bian Y Y, Chen D F, Peckmann J, Bohrmann G, Roberts H H. 2013. Rare earth elements of seep carbonates: indication for redox variations and microbiological processes at modern seep sites. *Journal of Asian Earth Sciences*, **65**: 27-33.

Franchi F, Rovere M, Gamberi F, Rashed H, Vaselli O, Tassi F. 2017. Authigenic minerals from the Paola Ridge (southern Tyrrhenian Sea): evidences of episodic methane seepage. *Marine and Petroleum Geology*, **86**: 228-247.

Freslon N, Bayon G, Toucanne S, Bermell S, Bollinger C, Chéron S, Etoubleau J, Germain Y, Khripounoff A, Ponzevera E, Rouget M L. 2014. Rare earth elements and neodymium isotopes in sedimentary organic matter. *Geochimica et Cosmochimica Acta*, **140**: 177-198.

Frisia S, Borsato A, Hellstrom J. 2018. High spatial resolution investigation of nucleation, growth and early diagenesis in speleothems as exemplar for sedimentary carbonates. *Earth-Science Reviews*, **178**: 68-91.

Glasby G P, Notsu K. 2003. Submarine hydrothermal mineralization in the Okinawa Trough, SW of Japan: an overview. *Ore Geology Reviews*, **23**(3-4): 299-339.

Greinert J, Bohrmann G, Suess E. 2001. Gas hydrate-associated carbonates and methane-venting at Hydrate Ridge: classification, distribution, and origin of Authigenic Lithologies. *In*: Paull C K, Dillon W P eds. Natural Gas Hydrates: Occurrence, Distribution, and Detection. American Geophysical Union, Washington. p.99-113.

Guo K, Zhai S K, Yu Z H, Cai Z W, Zhang X. 2016. Determination and tectonic significance of volcanic rock series in the Okinawa Trough. *Earth Science*, **41**(10): 1655-1664. (in Chinese with English abstract)

Han X Q, Suess E, Huang Y Y, Wu N Y, Bohrmann G, Su X, Eisenhauer A, Rehder G, Fang Y X. 2008. Jiulong methane reef: microbial mediation of seep carbonates in the South China Sea. *Marine Geology*, **249**(3-4): 243-256.

Himmler T, Bach W, Bohrmann G, Peckmann J. 2010. Rare earth elements in authigenic methane-seep carbonates as tracers for fluid composition during early diagenesis. *Chemical Geology*, **277**(1-2): 126-136.

Himmler T, Haley B A, Torres M E, Klinkhammer G P, Bohrmann G, Peckmann J. 2013. Rare earth element geochemistry in cold-seep pore waters of Hydrate Ridge, northeast Pacific Ocean. *Geo-Marine Letters*, **33**(5): 369-379.

Irwin H, Curtis C, Coleman M. 1977. Isotopic evidence for source of diagenetic carbonates formed during burial of organic-rich sediments. *Nature*, **269**(5625): 209-213.

James N P, Choquette P W. 1983. Limestones: the sea floor diagenetic environment. *Diagenesis*: *Geoscience Canada Serial*, **10**(2): 162-179.

Jin X L, Yu P Z. 1987. Tectonic characteristics and evolution of the Okinawa Trough. *Science in China Series B*, (2): 196-203. (in Chinese)

Joseph C, Campbell K A, Torres M E, Martin R A, Pohlman J W, Riedel M, Rose K. 2013. Methane-derived authigenic carbonates from modern and paleoseeps on the Cascadia margin: Mechanisms of formation and diagenetic signals. *Palaeogeography*, *Palaeoclimatology*, *Palaeoecology*, **390**: 52-67.

Li J W, Peng X T, Bai S J, Chen Z Y, Van Nostrand J D. 2018. Biogeochemical processes controlling authigenic carbonate formation within the sediment column from the Okinawa Trough. *Geochimica et Cosmochimica Acta*, **222**: 363-382.

Liebetrau V, Eisenhauer A, Linke P. 2010. Cold seep carbonates and associated cold-water corals at the Hikurangi Margin, New Zealand: new insights into fluid pathways, growth structures and geochronology. *Marine Geology*, **272**(1-4): 307-318.

Lin Q, Wang J S, Algeo T J, Sun F, Lin R X. 2016. Enhanced framboidal pyrite formation related to anaerobic oxidation of methane in the sulfate-methane transition zone of the

northern South China Sea. *Marine Geology*, **379**: 100-108.

Liu G D. 1989. Geophysical and geological exploration and hydrocarbon prospects of the East China Sea. *China Earth Sciences*, **1**(1): 43-58.

Luan X W, Lu Y T, Zhao K B, Sun D S, Li J. 2008. Geological factors for the development and newly advances in exploration of gas hydrate in East China Sea slope and Okinawa Trough. Geoscience, **22**(3): 342-355. (in Chinese with English abstract)

Luff R, Wallmann K, Aloisi G. 2004. Numerical modeling of carbonate crust formation at cold vent sites: significance for fluid and methane budgets and chemosynthetic biological communities. *Earth and Planetary Science Letters*, **221**(1-4): 337-353.

Lumsden D N. 1979. Discrepancy between thin-section and X-ray estimates of dolomite in limestone. *Journal of Sedimentary Research*, **49**(2): 429-435.

Magalhães V H, Pinheiro L M, Ivanov M K, Kozlova E, Blinova V, Kolganova J, Vasconcelos C, Mckenzie J A, Bernasconi S M, Kopf A J, Díaz-Del-Río V, González F J, Somoza L. 2012. Formation processes of methane-derived authigenic carbonates from the Gulf of Cadiz. *Sedimentary Geology*, **243-244**: 155-168.

Mazzini A, Ivanov M K, Parnell J, Stadnitskaia A, Cronin B T, Poludetkina E, Mazurenko L, Van Weering T C E. 2004. Methane-related authigenic carbonates from the Black Sea: geochemical characterisation and relation to seeping fluids. *Marine Geology*, **212**(1-4): 153-181.

McLennan S M. 1989. Rare earth elements in sedimentary rocks: influence of provenance and sedimentary processes. *Reviews in Mineralogy and Geochemistry*, **21**(1): 169-200.

Moore T S, Murray R W, Kurtz A C, Schrag D P. 2004. Anaerobic methane oxidation and the formation of dolomite. *Earth and Planetary Science Letters*, **229**(1-2): 141-154.

Morse J W. 2003. Formation and diagenesis of carbonate sediments. *Treatise on Geochemistry*, **7**: 67-85.

Naehr T H, Eichhubl P, Orphan V J, Hovland M, Paull C K, Ussler III W, Lorenson T D, Greene H G. 2007. Authigenic carbonate formation at hydrocarbon seeps in continental margin sediments: a comparative study. *Deep Sea Research Part II*: *Topical Studies in Oceanography*, **54**(11-13): 1268-1291.

Nöthen K, Kasten S. 2011. Reconstructing changes in seep activity by means of pore water and solid phase Sr/Ca and Mg/Ca ratios in pockmark sediments of the Northern Congo Fan. *Marine Geology*, **287**(1-4): 1-13.

Panieri G, Camerlenghi A, Cacho I, Cervera C S, Canals M, Lafuerza S, Herrera G. 2012. Tracing seafloor methane emissions with benthic foraminifera: results from the Ana submarine landslide (Eivissa Channel, Western Mediterranean Sea). *Marine Geology*, **291-294**: 97-112.

Peckmann J, Reimer A, Luth U, Luth C, Hansen B T, Heinicke C, Hoefs J, Reitner J. 2001. Methane-derived carbonates and authigenic pyrite from the northwestern Black Sea. *Marine Geology*, **177**(1-2): 129-150.

Peng X T, Guo Z X, Chen S, Sun Z L, Xu H C, Ta K W, Zhang J C, Zhang L J, Li J W, Du M R. 2017. Formation of carbonate pipes in the northern Okinawa Trough linked to strong sulfate exhaustion and iron supply. *Geochimica et Cosmochimica Acta*, **205**: 1-13.

Pierre C, Blanc-Valleron M M, Demange J, Boudouma O, Foucher J P, Pape T, Himmler T, Fekete N, Spiess V. 2012. Authigenic carbonates from active methane seeps offshore southwest Africa. *Geo-Marine Letters*, **32**(5): 501-513.

Pierre C, Fouquet Y. 2007. Authigenic carbonates from methane seeps of the Congo deep-sea fan. *Geo-Marine Letters*, **27**(2-4): 249-257.

Pierre C. 2017. Origin of the authigenic gypsum and pyrite from active methane seeps of the southwest African Margin. *Chemical Geology*, **449**: 158-164.

Roberts H H, Aharon P. 1994. Hydrocarbon-derived carbonate buildups of the northern Gulf of Mexico continental slope: a review of submersible investigations. *Geo-Marine Letters*, **14**(2-3): 135-148.

Rongemaille E, Bayon G, Pierre C, Bollinger C, Chu N C, Fouquet Y, Riboulot V, Voisset M. 2011. Rare earth elements in cold seep carbonates from the Niger delta. *Chemical Geology*, **286**(3-4): 196-206.

Sackett W M. 1978. Carbon and hydrogen isotope effects during the thermocatalytic production of hydrocarbons in laboratory simulation experiments. *Geochimica et Cosmochimica Acta*, **42**(6): 571-580.

Shields G, Stille P. 2001. Diagenetic constraints on the use of cerium anomalies as palaeoseawater redox proxies: an isotopic and REE study of Cambrian phosphorites. *Chemical Geology*, **175**(1-2): 29-48.

Sibuet J C, Deffontaines B, Hsu S K, Thareau N, Le Formal J P, Liu C S. 1998. Okinawa trough backarc basin: early tectonic and magmatic evolution. *Journal of Geophysical Research*: *Solid Earth*, **103**(B12): 30245-30267.

Smrzka D, Feng D, Himmler T, Zwicker J, Hu Y, Monien P, Tribovillard N, Chen D, Peckmann J. 2020. Trace elements in methane-seep carbonates: potentials, limitations, and perspectives. *Earth-Science Reviews*, **208**: 103263.

Suess E. 2014. Marine cold seeps and their manifestations: geological control, biogeochemical criteria and environmental conditions. *International Journal of Earth Sciences*, **103**(7): 1889-1916.

Sun Z L, Wei H L, Zhang X H, Shang L N, Yin X J, Sun Y B, Xu L, Huang W, Zhang X R. 2015. A unique Fe-rich carbonate chimney associated with cold seeps in the Northern Okinawa Trough, East China Sea. *Deep Sea Research Part I*: *Oceanographic Research Papers*, **95**: 37-53.

Sun Z L, Wu N Y, Cao H, Xu C L, Liu L P, Yin X J, Zhang X R, Geng W, Zhang X L. 2019. Hydrothermal metal supplies enhance the benthic methane filter in oceans: an example from the Okinawa Trough. *Chemical Geology*, **525**: 190-209.

Swart P K, Oehlert A M. 2018. Revised interpretations of

stable C and O patterns in carbonate rocks resulting from meteoric diagenesis. *Sedimentary Geology*, **364**: 14-23.

Swart P K. 2015. The geochemistry of carbonate diagenesis: the past, present and future. *Sedimentology*, **62**(5): 1233-1304.

Tong H P, Wang Q X, Peckmann J, Cao Y C, Chen L Y, Zhou W D, Chen D F. 2016. Diagenetic alteration affecting $\delta^{18}O$, $\delta^{13}C$ and $^{87}Sr/^{86}Sr$ signatures of carbonates: a case study on cretaceous seep deposits from Yarlung-Zangbo Suture Zone, Tibet, China. *Chemical Geology*, **444**: 71-82.

Wang Q X, Tong H P, Huang C Y, Chen D F. 2018. Tracing fluid sources and formation conditions of Miocene hydrocarbon-seep carbonates in the central Western Foothills, Central Taiwan. *Journal of Asian Earth Sciences*, **168**: 186-196.

Wang S H, Yan W, Chen Z, Zhang N, Chen H. 2014. Rare earth elements in cold seep carbonates from the southwestern Dongsha area, northern South China Sea. *Marine and Petroleum Geology*, **57**: 482-493.

Warthmann R, Van Lith Y, Vasconcelos C, McKenzie J A, Karpoff A M. 2000. Bacterially induced dolomite precipitation in anoxic culture experiments. *Geology*, **28**(12): 1091-1094.

Whiticar M J. 1999. Carbon and hydrogen isotope systematics of bacterial formation and oxidation of methane. *Chemical Geology*, **161**(1-3): 291-314.

Wright J, Schrader H, Holser W T. 1987. Paleoredox variations in ancient oceans recorded by rare earth elements in fossil apatite. *Geochimica et Cosmochimica Acta*, **51**(3): 631-644.

Wu B H, Zhang G X, Zhu Y H, Lu Z Q, Chen B Y. 2003. Progress of gas hydrate investigation in China offshore. *Earth Science Frontiers*, **10**(1): 177-189. (in Chinese with English abstract)

Wu N Y, Sun Z L, Lu J G, Cai F, Cao H, Geng W, Luo M, Zhang X L, Li Q, Shang L N, Wang L B, Zhang X R, Xu C L, Zhai B, Li X, Gong J M, Hu Y, Lin G M. 2019. Interaction between seafloor cold seeps and adjacent hydrothermal activities in the Okinawa Trough. *Marine Geology & Quaternary Geology*, **39**(5): 23-35. (in Chinese with English abstract)

Wu Z Y, Li J B, Jin X L, Shang J H, Li S J, Jin X B. 2014. Distribution, features, and influence factors of the submarine topographic boundaries of the Okinawa Trough. *Science China Earth Sciences*, **57**(8): 1885-1896.

Xu N, Wu S G, Wang X J, Guo J H. 2006. Seismic study of the gas hydrate in the continental slope of the Okinawa Trough, East China Sea. *Progress in Geophysics*, **21**(2): 564-571. (in Chinese with English abstract)

Yang K H, Zhu Z Z, Dong Y H, Chu F Y, Zhang W Y, 2021. Evolution and diagenetic implications of framboids in the methane-related carbonates of the northern Okinawa Trough. *Acta Oceanologica Sinica*, **40**(12): 114-124.

Zhao D B, Wan S M. 2015. Research progress of tracing sediment sources in Okinawa Trough. *Marine Geology Frontiers*, **31**(2): 32-41. (in Chinese with English abstract)

Zwicker J, Smrzka D, Himmler T, Monien P, Gier S, Goedert J L, Peckmann J. 2018. Rare earth elements as tracers for microbial activity and early diagenesis: a new perspective from carbonate cements of ancient methane-seep deposits. *Chemical Geology*, **501**: 77-85.